

1 **Contrasting size-resolved hygroscopicity of fine particles derived by HTDMA and HR-AMS**  
2 **measurements between summer and winter in urban Beijing: the impacts of aerosol aging and local**  
3 **emissions on its hygroscopicity**

4 Xinxin Fan<sup>1\*</sup>, Jieyao Liu<sup>1\*</sup>, Fang Zhang<sup>1#</sup>, Lu Chen<sup>1</sup>, Don Collins<sup>2</sup>, Weiqi Xu<sup>3,4</sup>, Xiaoi Jin<sup>1</sup>, Jingye  
5 Ren<sup>1</sup>, Yuying Wang<sup>1,5</sup>, Hao Wu<sup>1</sup>, Shangze Li<sup>1</sup>, Yele Sun<sup>3,4</sup>, Zhanqing Li<sup>1,6</sup>

6  
7 <sup>1</sup>*State Key Laboratory of Earth Surface Processes and Resource Ecology, College of Global Change and*  
8 *Earth System Science, Beijing Normal University, Beijing 100875, China*

9 <sup>2</sup>*Department of Chemical and Environmental Engineering, University of California Riverside, Riverside,*  
10 *California, USA*

11 <sup>3</sup>*State Key Laboratory of Atmospheric Boundary Layer Physics and Atmospheric Chemistry, Institute of*  
12 *Atmospheric Physics, Chinese Academy of Sciences, Beijing 100029, China*

13 <sup>4</sup>*College of Earth Sciences, University of Chinese Academy of Sciences, Beijing 100049, China*

14 <sup>5</sup>*School of Atmospheric Physics, Nanjing University of Information Science and Technology, Nanjing*  
15 *210044, China*

16 <sup>6</sup>*Earth System Science Interdisciplinary Center and Department of Atmospheric and Oceanic Science,*  
17 *University of Maryland, College Park, Maryland, USA*

18 \*Those authors contribute equally to this work

19  
20 #Correspondence to: [Fang.zhang@bnu.edu.cn](mailto:Fang.zhang@bnu.edu.cn)

21 **Abstract**

22 The effects of aerosols on visibility through scattering and absorption of light and on climate through  
23 altering cloud droplet concentration are closely associated with their hygroscopic properties. Here, based on  
24 field campaigns in winter and summer in Beijing, we compare the size-resolved hygroscopic parameter ( $\kappa_{gf}$ )  
25 of ambient fine particles derived by an HTDMA (Hygroscopic Tandem Differential Mobility Analyzer) to  
26 that (denoted as  $\kappa_{chem}$ ) of calculated by an HR-ToF-AMS (High-resolution Time-of-Flight Aerosol Mass  
27 Spectrometer) measurements using a simple rule with the hypothesis of uniform internal mixing of aerosol  
28 particles. We mainly focus on contrasting the disparity of  $\kappa_{gf}$  and  $\kappa_{chem}$  between summer and winter to reveal  
29 the impact of atmospheric processes/emission sources on aerosols hygroscopicity and to evaluate the  
30 uncertainty in estimating particles hygroscopicity with the hypothesis. We show that, in summer, the  $\kappa_{chem}$   
31 for 110, 150 and 200 nm particles was on average ~10% - 12% lower than  $\kappa_{gf}$ , with the greatest difference  
32 between the values observed around noontime when aerosols experience rapid photochemical aging. In

winter, no apparent disparity between  $\kappa_{chem}$  and  $\kappa_{gf}$  is observed for those >100 nm particles around noontime, but the  $\kappa_{chem}$  is much higher than  $\kappa_{gf}$  in the late afternoon when ambient aerosols are greatly influenced by local traffic and cooking sources. By comparing with the observation from other two sites (Xingtai, Hebei and Xinzhou, Shanxi) of north China, we verify that atmospheric photochemical aging of aerosols enhances their hygroscopicity and leads to 10%-20% underestimation in  $\kappa_{chem}$  if using the uniform internal mixing assumption. The effect is found more significant for these >100 nm particles observed in remote or clean regions. The lower  $\kappa_{chem}$  is likely resulted from multiple impacts of inappropriate application of density and hygroscopic parameter of organic aerosols in the calculation, as well as influences from chemical interaction between organic and inorganic compounds on the overall hygroscopicity of mixed particles. We also find that, local/regional primary emissions, which result in a large number of externally-mixed BC and POA (Primary Organic Aerosol) in urban Beijing during traffic rush hour time, cause 20-40% overestimation of the hygroscopic parameter. This is largely due to an inappropriate use of density of the BC particles that is closely associated with its morphology or degree of its aging. The results show that the calculation can be improved by applying an effective density of freshly BC (0.25-0.45 g cm<sup>-3</sup>) in the mixing rule assumption. Our study suggest that it is critical to measure the effective density and morphology of ambient BC in particularly in those regions with influences of rapid secondary conversion/aging processes and local sources, so as to accurately parameterize the effect of BC aging on particles hygroscopicity.

## 1. Introduction

The effects of aerosols on visibility through scattering and absorption of light and on climate through altering cloud droplet concentration are influenced by their hygroscopic growth. Understanding and reducing the uncertainty in prediction of the aerosol hygroscopic parameter ( $\kappa$ ) using chemical composition would improve model predictions of aerosol effects on clouds and climate.

The hygroscopic properties of both the natural and anthropogenic aerosols, in addition to being affected by its chemical composition (Gunthe et al., 2009), are also affected by the particle mixing state and aging (Schill et al., 2015; Peng et al., 2017a). For example, a recent laboratory study showed that the coexisting hygroscopic species have a strong influence on the phase state of particles, thus affecting chemical

59 interactions between inorganic and organic compounds as well as the overall hygroscopicity of mixed  
60 particles (Peng et al., 2016a). The field measurements also demonstrated that the hydrophobic black carbon  
61 particles became hygroscopic with atmospheric mixing and aging by organics (i.e. Peng et al., 2017a). In a  
62 heavily polluted atmosphere with varied aerosol sources and sinks as well as complex physical and chemical  
63 processes, the mixing state and its impact on aerosols hygroscopicity is more complicated. The  
64 hygroscopicity of mixed particles and mutual impacts between the components are still poorly understood.

65 Previous studies have shown that the difference between the  $\kappa$  obtained from H-TDMA or CCNc  
66 measurements and calculated based on the volume mixing ratio of chemical components. Laboratory results  
67 from Cruz and Pandis (2000) indicate that  $\kappa_{gf}$  of internally mixed ammonium sulfate and organic matter is  
68 higher than  $\kappa_{chem}$  calculated for assumed uniform internal mixing. But Peng et al (2016a) found that, for  
69 sodium chloride and organic aerosols mixed particles, the measured growth factors by H-TDMA were  
70 significantly lower than calculations from the mixing rule methods. In some field studies on aged aerosols,  
71 the  $\kappa$  was underestimated by the calculation based on uniform internal mixing assumption and thus lead to  
72 an underestimation of CCN concentration (Bougiatioti, et al., 2009; Chang, et al., 2007; Kuwata, et al., 2008;  
73 Wang, et al., 2010; Ren et al., 2018). However, during primary emission dominated periods, the  $\kappa$  value  
74 from calculations based on bulk chemical composition was much higher than that measured by H-TDMA  
75 measurements (Zhang et al., 2017). The various results from previous studies suggest distinct effects of  
76 aerosols mixing state on their hygroscopicity. Overall, to what extent do the differences depend on the  
77 mixing state and the extent of aging of the particles, and how the different atmospheric processes and what  
78 kinds of mixing structure of the particles may result in those disparity between measured and calculated  
79 hygroscopic parameter have not been clearly clarified by the previous studies. A comprehensive  
80 investigation on the causes and magnitude of the effect is with great significance to parameterize the effect  
81 of atmospheric processes/emissions of aerosols on particles hygroscopicity in models.

82 In the atmosphere, the  $\kappa$ , which is related to the particle mixing state diversity, varies largely across the  
83 size range of ambient fine particles (Rose et al., 2010). However, previous study just compared the  $\kappa$   
84 calculated from bulk chemical composition to that measured by H-TDMA (Zhang et al., 2017). Using  
85 size-resolved, not bulk chemical composition measurements in different seasons, is expected to provide

86 more comprehensive understanding and insights of how the aerosols mixing state influence on their  
87 hygroscopicity, motivating our analysis that employs size-resolved chemical composition measured by an  
88 HR-ToF-AMS in this study. The aim of this paper is to study the hygroscopicity and mixing state  
89 characteristics of fine particles in the Beijing urban area, and to reveal the impact of atmospheric  
90 processes/sources and mixing/aging on aerosols hygroscopicity and elucidate the uncertainty in calculating  
91 the hygroscopic parameter using simple mixing rule estimates based on size-resolved chemical composition.  
92 The experiment and theory in the study are introduced in Sect. 2. The comparison between the hygroscopic  
93 parameter obtained from the HTDMA and that calculated using size-resolved chemical composition is  
94 discussed in Sect. 3. Conclusions from the study are given in Sect. 4.

## 95 **2. Experiment and Theory**

### 96 **2.1. Site and instruments**

97 Two field campaigns are conducted during winter 2016 and summer 2017 of urban Beijing (Fig. 1, BJ:  
98 39.97 °N, 116.37 °E) for measurements of aerosols physical and chemical properties. The BJ site is located  
99 at the Institute of Atmospheric Physics (IAP), Chinese Academy of Sciences, which is between the north  
100 third and fourth ring roads in northern Beijing. Local traffic and cooking emissions can be important at the  
101 site (Sun et al., 2015). The sampling period in cold season was from 16 November to 10 December 2016,  
102 during the domestic heating period in Beijing. The sampling period in warm season was from 25 May to 18  
103 June 2017.

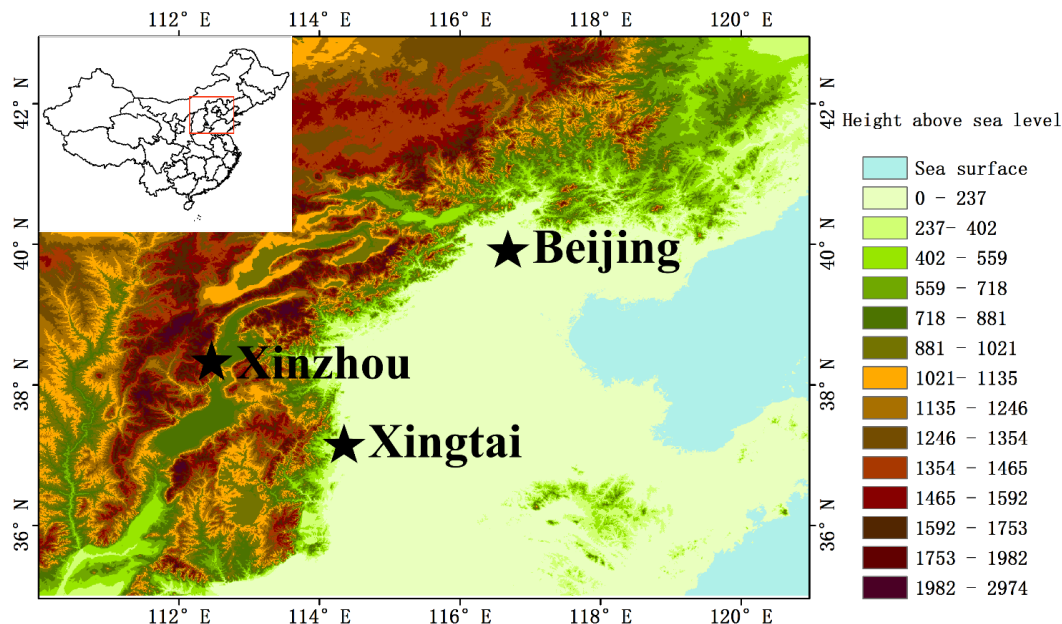


Figure 1. The map location of the sites

Particle number size distribution (PNSD) in the size range from 10 nm to 550 nm was measured with a Scanning Mobility Particle Sizer (SMPS; Wang & Flagan, 1990; Collins et al., 2002), which consists of a long differential mobility analyzer (DMA, model 3081L, TSI Inc) to classify the particle and a condensation particle counter (CPC, model 3772, TSI Inc.) to detect the size classified particles. The sampled particles were dried to relative humidity < 30% before entering the DMA. The measurement time for each size distribution was five minutes.

The HTDMA system used in this study has been described in detail in previous publications (Tan et al., 2013; Wang et al., 2017; Zhang et al., 2017). Here, only a brief description is given. A Nafion dryer dried the sampled particles to relative humidity < 20%, after which the steady state charge distribution was reached in a bipolar neutralizer. The first differential mobility analyzer (DMA<sub>1</sub>, model 3081L, TSI Inc.) selected the quasi-monodisperse particles through applying a fixed voltage. The dry diameters selected in this study were 40, 80, 110, 150, and 200 nm. The quasi-monodisperse particles were humidified to a controlled RH (90% in this study) using a Nafion humidifier. A second DMA (DMA<sub>2</sub>, same model as the DMA<sub>1</sub>) coupled with a water-based condensation particle counter (WCPC, model 3787, TSI Inc.) measured

121 the particle number size distributions of the humidified aerosol. RH calibration with ammonium sulfate was  
122 carried out regularly during the study.

123 The hygroscopic growth factor (Gf) is defined as the ratio of the mobility diameter at a given RH to the  
124 dry diameter:

$$Gf = \frac{D(RH)}{D(dry)}$$

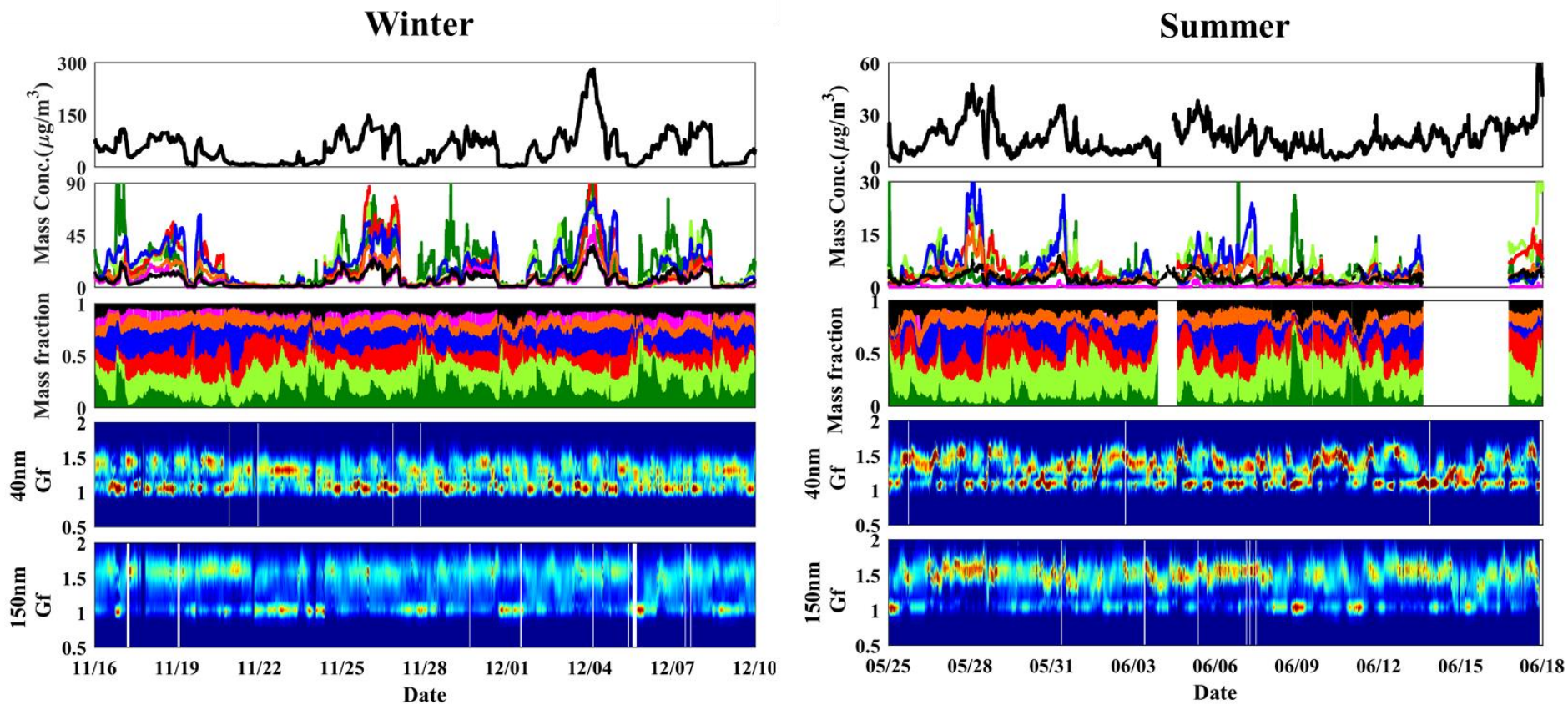
125 The Gf probability density function (PDF) is retrieved based on the TDMA<sub>inv</sub> algorithm developed by  
126 Gysel et al. (2009). Dry scans in which the RH between the two DMAs was not increased were used to  
127 define the width of the transfer function.

128 Size-resolved non-refractory submicron aerosol composition was measured with an Aerodyne  
129 high-resolution time-of-flight aerosol mass spectrometer (HR-ToF-AMS; Xu et al., 2015). The particle  
130 mobility diameter was estimated by dividing the vacuum aerodynamic diameter from the AMS  
131 measurements by particle density. Because the uncertainty caused by the fixed density across the size range  
132 is negligible (Wang et al. 2016), here, the particle density is assumed to be 1600 kg m<sup>-3</sup> (Hu et al., 2012).  
133 AMS positive matrix factorization (PMF) with the PMF2.exe (v4.2) method was performed to identify  
134 various factors of organic aerosols. Xu et al. (2015) have described the operation and calibration of the  
135 HR-ToF-AMS in detail. Black carbon (BC) mass concentration was derived from measurements of light  
136 absorption with a 7-wavelength aethalometer (AE33, Magee Scientific Corp.; Zhao et al., 2017).

## 137 **2.2. Data**

138 The time series of the submicron particle mass concentration PM<sub>1</sub>, bulk mass concentrations of the  
139 main species in PM<sub>1</sub>, mass fraction of the chemical composition of PM<sub>1</sub>, and probability density function of  
140 growth factor (Gf-PDFs) for 40 and 150 nm particles during the campaign are presented in Fig. 2. Quite  
141 distinct temporal variability of aerosol chemical and physical properties was observed between winter and  
142 summer. The average mass concentration of PM<sub>1</sub> was 55.2 µg/m<sup>3</sup> in the winter and 16.5 µg/m<sup>3</sup> in the  
143 summer during our study periods. In this study, we define the conditions when the mass concentration in  
144 winter period was < 20 µg m<sup>-3</sup> and >80 µg m<sup>-3</sup> as clean and polluted conditions, respectively. Organic

145 aerosol (OA), consisting of secondary organic aerosol (SOA) and primary organic aerosol (POA), was the  
146 major fraction during both the winter and summer sampling periods. POA concentration was higher than  
147 that of SOA in the winter, which reflects the influence of primary emissions such as coal combustion OA  
148 (COOA) in Beijing (Hu et al., 2016; Sun et al., 2016). In contrast, SOA usually dominated in the summer,  
149 which is evident that secondary aerosol formation played a key role in the source of  $PM_{10}$ . Distinct  
150 hydrophobic (with Gf of  $\sim 1.0$ ) and more hygroscopic (with Gf of  $\sim 1.5$ ) modes were observed from Gf-PDFs  
151 of both small and large particles. Sometimes the more hygroscopic mode particles were more concentrated  
152 and at others the hydrophobic particles were. In general though, the more hygroscopic mode dominated for  
153 larger particles (i.e. 150 nm), and the less hygroscopic mode did for the smallest particles (e.g. 40 nm).  
154 Occasionally, only the hydrophobic mode was evident for 150 nm particles, which occurred when POA  
155 dominated the  $PM_{10}$ . Only the hygroscopic mode was discernable for 40 nm particles during new particle  
156 formation (NPF) events that occurred more frequently in summer than winter (Fig. 3).



157

158

159

Figure 2. Winter (left) and summer (right) time series of mass concentration of  $\text{PM}_{10}$ , bulk mass concentration of the main species in  $\text{PM}_{10}$ , mass fraction of the chemical composition of  $\text{PM}_{10}$  and Gf-PDFs for 40 and 150 nm particles.



## 2.3. Theory and method

### 2.3.1 Derivation of the hygroscopic parameter, $\kappa$ , from the growth factor (Gf)

According to  $\kappa$ -Köhler Theory (Petters and Kreidenweis, 2007), the hygroscopicity parameter  $\kappa$  can be derived using the growth factor measured by an HTDMA.

$$\kappa = (Gf^3 - 1) \left( \frac{\exp\left(\frac{A}{D_d Gf}\right)}{RH} - 1 \right), \quad (1)$$

$$A = \frac{4\sigma_{s/a} M_w}{RT\rho_w}, \quad (2)$$

where Gf is hygroscopic growth factor measured by HTDMA,  $D_d$  is the dry diameter of the particles, RH is the relative humidity in the HTDMA (90%, in our study),  $\sigma_{s/a}$  is the surface tension of the solution/air (assumed here to be the surface tension of pure water,  $\sigma_{s/a} = 0.0728 \text{ N m}^{-2}$ ),  $M_w$  is the molecular weight of water, R is the universal gas constant, T is the absolute temperature, and  $\rho_w$  is the density of water.

### 2.3.2 Derivation of the hygroscopic parameter, $\kappa$ , from chemical composition data

For an assumed internal mixture,  $\kappa$  can also be calculated by a simple mixing rule on the basis of chemical volume fractions (Petters and Kreidenweis, 2007; Gunthe et al., 2009):

$$\kappa_{chem} = \sum_i \varepsilon_i \kappa_i, \quad (3)$$

where  $\kappa_i$  and  $\varepsilon_i$  are the hygroscopicity parameter and volume fraction for the individual (dry) component in the mixture, respectively. The AMS provides mass concentrations of organics and of many inorganic ions. The inorganic components mainly consisted of  $(\text{NH}_4)_2\text{SO}_4$  and  $\text{NH}_4\text{NO}_3$  (Zhang et al., 2014). And the values of  $\kappa$  are 0.48 for  $(\text{NH}_4)_2\text{SO}_4$  and 0.58 for  $\text{NH}_4\text{NO}_3$  (Petters and Kreidenweis, 2007). To estimate  $\kappa_{org}$ , we used the following linear function derived by Mei et al. (2013):  $\kappa_{org} = 2.10 \times f_{44} - 0.11$ . We derived the volume fraction of each species by dividing mass concentration by its density. The density are  $1.77 \text{ g cm}^{-3}$

180 for  $(\text{NH}_4)_2\text{SO}_4$  and  $1.72 \text{ g cm}^{-3}$  for  $\text{NH}_4\text{NO}_3$ . The densities of organics are assumed to be  $1.2 \text{ g cm}^{-3}$  (Turpin  
181 et al., 2001). The  $\kappa$  and density of BC are assumed to be 0 and  $1.7 \text{ g cm}^{-3}$ . In the following discussions,  $\kappa_{gf}$   
182 and  $\kappa_{\text{chem}}$  denote the values derived from HTDMA measurements and calculated using the ZSR mixing rule,  
183 respectively.

184 In addition, we also compare the results from the field campaigns with those from other two sites,  
185 Xingtai (XT:  $37.18^\circ\text{N}$ ,  $114.37^\circ\text{E}$ ), and Xinzhou (XZ:  $38.24^\circ\text{N}$ ,  $112.43^\circ\text{E}$ ), in North China Plain (Fig. 1).  
186 At XZ site, we use the hygroscopic parameter (defined as  $\kappa_{CCNc}$ ) from size-resolved CCN measurements  
187 (Zhang et al., 2014, 2016) for comparison. More detailed descriptions of the method to retrieve  $\kappa_{CCNc}$  can be  
188 found in (Petters and Kreidenweis (2007)). Both of the  $\kappa_{gf}$  and  $\kappa_{CCNc}$  are derived based on  $\kappa$ -Köhler Theory  
189 (Petters and Kreidenweis, 2007). But, different from the  $\kappa_{gf}$  measured by the HTDMA system which is  
190 operated at RH of 90%, the  $\kappa_{CCNc}$  is derived by measuring aerosols CCN activity under the condition of  
191 supersaturations with relative humidity of  $>100\%$ . Previous studies from field measurements and laboratory  
192 experiments showed that the  $\kappa_{CCNc}$  is generally slight larger or smaller than  $\kappa_{gf}$ , but they are basically  
193 comparable and can well represent an overall aerosols hygroscopicity (e.g. Carrico et al., 2008; Wex et al.,  
194 2009; Good et al., 2010; Irwin et al., 2010; Cerully et al., 2011; Wu et al., 2013; Zhang et al., 2017).

### 195 **3. Results and discussion**

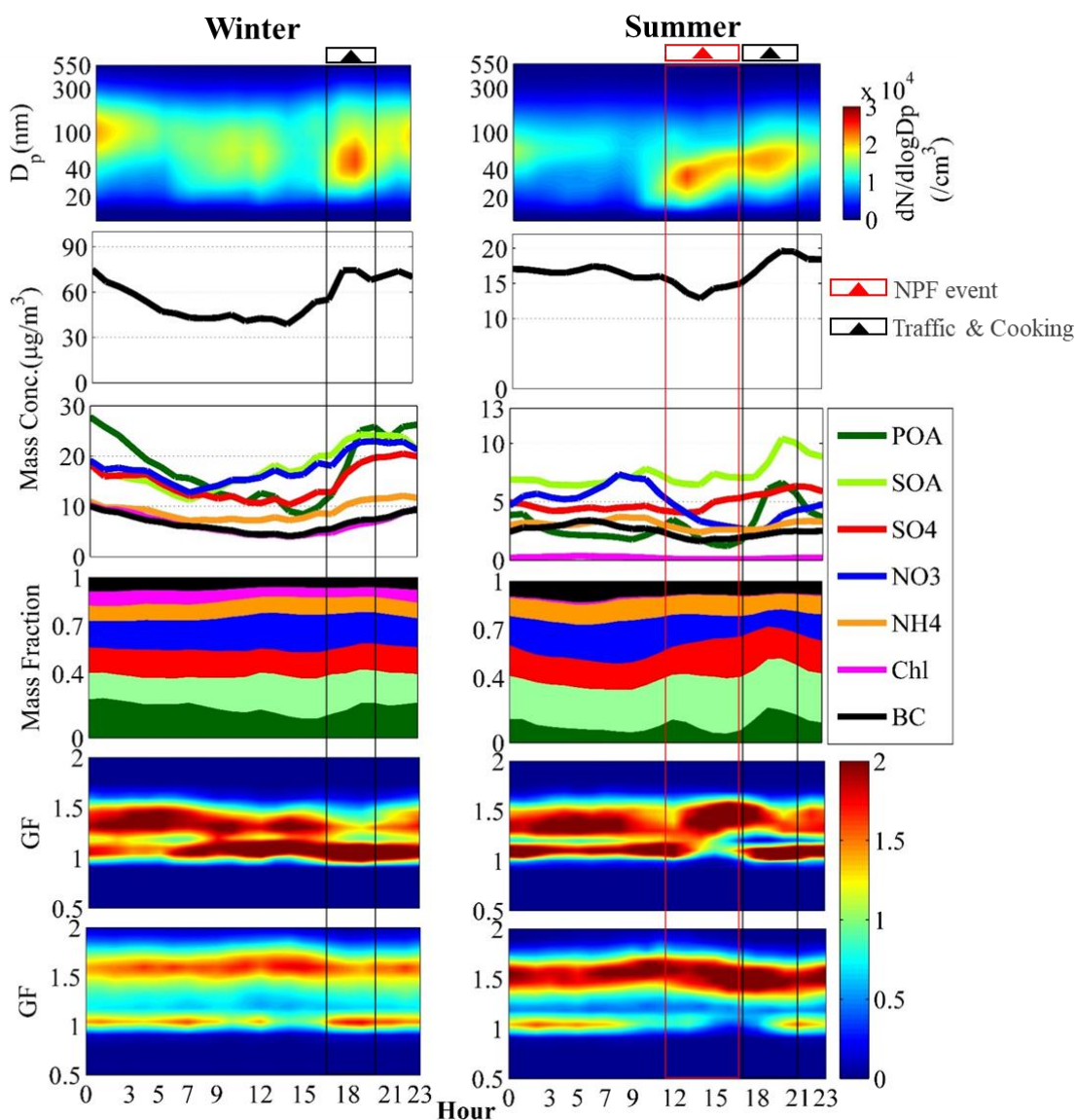
#### 196 **3.1. Diurnal variations of ambient fine particles physiochemical properties and hygroscopic growth** 197 **factor**

198 The diurnal variations of the PNSD, mass concentration of  $\text{PM}_{10}$ , mass concentration and fraction of  
199 chemical components in  $\text{PM}_{10}$ , and Gf-PDFs for 40 and 150 nm particles during the campaign are shown in  
200 Fig. 3. During the summer an obvious peak value in the PNSD is observed around noontime due to NPF  
201 events that typically started around 10:00 LT (Local Time). The resulting sharp increase in number  
202 concentration of nucleation mode particles was followed by decreased concentration and a rapid growth in  
203 diameter of the particles along with increased mass concentration of SOA and sulfate in  $\text{PM}_{10}$ , indicating

204 strong photochemical and secondary formation processes during daytime in the summer (Peng et al., 2017b,  
205 Marked in red box in Fig. 3). In contrast, NPF was not evident during the winter period, which may in part  
206 be due to the much higher ( $\sim 3x$ )  $PM_{10}$  mass concentrations in the winter than in the summer. Note that peak  
207 values in number concentration and in mass concentrations of  $PM_{10}$  and POA occurred during the early  
208 evening (17:00-21:00, LT) indicating the strong impact of local sources from traffic emissions and cooking  
209 (Marked in black box in Fig. 3, Peng et al., 2014). In addition, the diurnal cycles of aerosol physical and  
210 chemical properties are also influenced by the diurnal changes in the planetary boundary layer (PBL) that  
211 leads to accumulation of particles during nighttime when higher values of both number and mass  
212 concentration were observed.

213 Owing to the continued local and primary emissions near the study site, the Gf-PDFs for 40 nm  
214 particles generally display a bimodal shape with more and less hygroscopic modes (with Gf of  $\sim 1.5$  and  $\sim$   
215 1.1 respectively) throughout the day both in winter and summer periods, indicating an external mixing state  
216 for the 40 nm particles. Note that, during nighttime and early morning in the winter, the more hygroscopic  
217 mode dominated and was shifted to higher Gf than during the daytime. This is thought to be due to  
218 heterogeneous/aqueous reactions on pre-existing primary small particles, and/or coagulation/condensation  
219 processes that are enhanced at night under lower ambient temperature and higher relative humidity, all of  
220 which result in a more hygroscopic and more internally-mixed aerosol (Liu et al., 2011; Massling et al.,  
221 2005; Ye et al., 2013; Wu et al., 2016; Wang et al., 2018a). Interestingly, in the summer period, the  
222 concentration of the hydrophilic mode increased quickly around noontime and in the early afternoon  
223 (12:00-16:00), with a corresponding decrease in the relative concentration of the hydrophobic mode, which  
224 likely indicates a transformation of the particles from externally to internally mixing state as a result of the  
225 species condensation from the photochemical reaction (Wu et al., 2016; Wang et al., 2017), resulting in an  
226 increase in particle hygroscopicity. In addition, it is evident that 40 nm particles after 12:00 were dominated  
227 by NPF (Fig. 3). Therefore, the increase of hydrophobic mode particles suggests that a large amount of  
228 hydrophilic particles are generated from NPF. For 150 nm particles, the hygroscopic mode in the Gf-PDF is  
229 more dominant during daytime in particular during the summer period when the strong solar radiation  
230 promotes photochemical aging and growth, thus producing a more internally-mixed aerosol. The dominant

231 hydrophobic mode at around 18:00 was observed both in winter and summer and reflects abundant traffic  
 232 emissions and cooking sources (primarily with POA) during the early evening period.

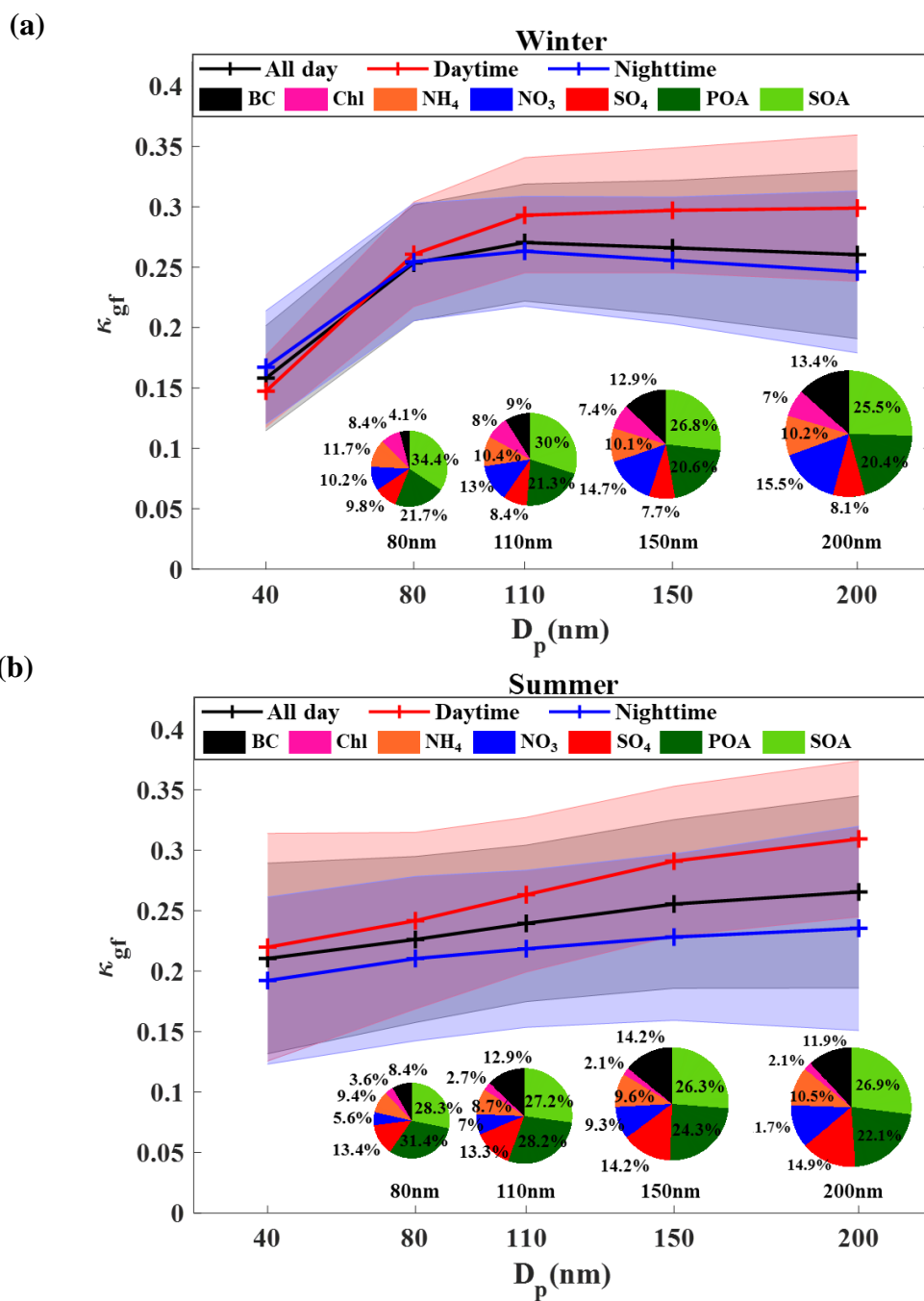


233  
 234 Figure 3. Campaign averaged diurnal variations in particle number size distribution; mass concentration of  
 235  $PM_{10}$ , bulk mass concentration of main species in  $PM_{10}$ , mass fraction of chemical composition of  $PM_{10}$ ; and  
 236 Gf-PDFs for 40 and 150 nm particles in winter (left panels) and summer (right panels) measured in urban  
 237 Beijing..

### 238 3.2 $\kappa_{gf}$ dependence on $D_p$

239 The size dependence of particle hygroscopicity parameters for the winter and summer periods are  
 240 presented in Fig.4. In the winter, the 40 nm particles were least hygroscopic and the hygroscopicity of larger

241 particles (>80 nm) displayed insignificant dependence on particle size. The size independence for the larger  
 242 particles is consistent with the observed similarity in mass fractions of inorganic and organic species across



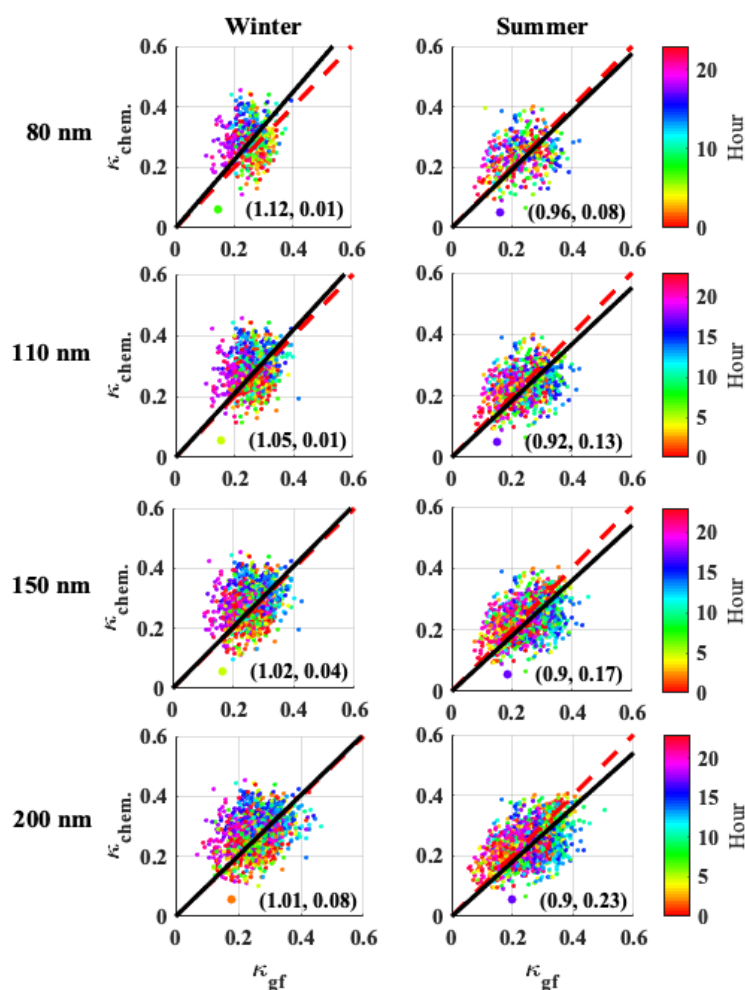
244  
 245 Figure 4. The dependence of  $\kappa$  on  $D_p$  at the urban Beijing site during winter (a) and summer (b). The  $\kappa$   
 246 values are retrieved from the size-resolved HTDMA measurements. The error bars represent  $\pm 1\sigma$ . The  
 247 size-resolved chemical mass fractions at the corresponding  $D_p$  is also presented.

248 the size range as shown in the pie charts in Figure 4a. A similar dependence of particle hygroscopicity on  
 249 particle size was also observed in the urban area of Beijing during the wintertime of 2014 (Wang et al.,

250 2018b). In the summer, hygroscopicity increased with increasing particle size, which is expected based on  
 251 the size dependent patterns shown in the pie charts, with the mass fraction of POA decreasing with the  
 252 particles size and the mass fraction of inorganics like sulfate and nitrate increasing with particle size.

### 253 3.3. Closure of HTDMA and chemical composition derived $\kappa$

254 A closure study was conducted between  $\kappa_{chem}$  and  $\kappa_{gf}$  (Fig. 5) to investigate the uncertainty of the two  
 255 methods, and especially to further illustrate whether particle hygroscopicity can be well predicted by  $\kappa_{chem}$   
 256 calculated by assuming internal mixing. Since a size-resolved BC mass concentration measurement was not



257  
 258 Figure 5. Closure of  $\kappa_{chem}$  calculated from size-resolved chemical composition data and  $\kappa_{gf}$  retrieved from  
 259 hygroscopic growth factor by HTDMA measurements in winter (left panels) and summer (right panels)  
 260 period. The dots with different color correspond to observed time of a day during the campaign as shown by  
 261 the color bar. On each plot, red dotted line is 1:1 line, black solid line is fitting line. The numbers in  
 262 parentheses are slopes of linear fits and correlation coefficients ( $R^2$ ).

263

264 available during the campaign, we use the bulk mass fraction of BC particles measured by the AE33  
265 combining with size-resolved BC distribution measured by a single particle soot photometer (SP2) in  
266 Beijing (Liu et al., 2018) to estimate  $\kappa_{chem}$ . During the calculation, the BC core diameter measured by SP2  
267 has been converted to the diameter of coated BC particles by multiplying factors of 1.4 and 2.6 under clean  
268 (with bulk BC mass concentrations  $<2 \mu\text{g m}^{-3}$ ) and polluted (with bulk BC mass concentrations  $>2 \mu\text{g m}^{-3}$ )  
269 conditions respectively (Liu et al., 2018).

270 Uncertainty in  $\kappa$  is due in part to measurement uncertainty of the HTDMA system and uncertainty  
271 resulting from non-ideality effects in the solution droplets, surface tension reduction due to surface active  
272 substances, and the presence of slightly soluble substances that dissolve at RH higher than that maintained in  
273 the HTDMA (e.g., Wex et al., 2009; Good et al., 2010; Irwin et al., 2010; Cerully et al., 2011; Wu et al.,  
274 2013). For example, the HTDMA may overestimate the  $D_p$  of dry particles for the external mixed BC  
275 particles, as BC-containing particles may shrink when humidified, leading to underestimate the hygroscopic  
276 growth factor. However, our previous study demonstrated that, for this region, estimates using HTDMA data  
277 are still better representing the aerosols hygroscopicity than those using the simple mixing rule based on  
278 chemical volume fractions for an assumed internal mixture (Zhang et al., 2017). Therefore, here we focus on  
279 discussing and exploring the uncertainty of  $\kappa_{chem}$  by taking  $\kappa_{gf}$  as the reference.

280 The results show that, although the slopes from linear fitting of  $\kappa_{chem}$  and  $\kappa_{gf}$  are close to 1.0, it is with  
281 quite poor correlations (typically with correlation coefficients,  $R^2$ , of  $< 0.3$ ) between  $\kappa_{chem}$  and  $\kappa_{gf}$  of the 80,  
282 110, 150, 200 nm particles both in winter and summer. The poor correlations reflect large uncertainty in one  
283 or both of the calculated parameters that are likely due to the unreasonable assumption of particle mixing  
284 state (e.g. Cruz and Pandis, 2000; Svenningsson et al., 2006; Sjogren et al., 2007; Zardini et al., 2008),  
285 which varies with their aging and other physiochemical processes in the atmosphere. Note that  
286 underestimation of  $\kappa_{chem}$  for the summer occurred mostly in the afternoon (Marked in blue dots in Fig. 5).  
287 This may be associated with photochemical processes at around noontime. More specific investigations of  
288 the particle mixing and aging impacts on  $\kappa_{chem}$  will be further addressed in the following sections.

### 3.4 Aerosols aging and sources effects indicated by diurnal cycles of $\kappa_{chem}$ and $\kappa_{gf}$

The diurnal cycles of particle hygroscopicity in the summer and winter with the use of the size-resolved chemical composition observations and the ratio of  $\kappa_{chem}$  to  $\kappa_{gf}$  are shown in Fig. 6. In summer, at 09:00-15:00, the disparity between  $\kappa_{chem}$  and  $\kappa_{gf}$  is insignificant for smaller particles (80 and 110 nm), both of them show slight decrease from 09:00 or 10:00 to 12:00-13:00 due to the frequent NPF event that usually corresponds to a large fraction of organics (Fig. 3) in urban Beijing. For larger particles (150 and 200 nm), the disparity between  $\kappa_{chem}$  and  $\kappa_{gf}$  around noontime and in the early afternoon is very significant, corresponding to >20% underestimation of particle hygroscopicity by  $\kappa_{chem}$  (with the ratio of  $\kappa_{chem}$  to  $\kappa_{gf}$  of ~0.8). Similar patterns were also noted by Zhang et al., (2017) but which is only based on a comparison between  $\kappa_{chem}$  derived from bulk chemical composition and  $\kappa_{gf}$ . Our results based on size-resolved measurements are consistent with that observed by Zhang et al., (2017), and thus again confirming an effect of the rapid photochemical aging of aerosol particles on their hygroscopicity. While, no significant differences between  $\kappa_{chem}$  and  $\kappa_{gf}$  are observed during night time in summer. Note that  $\kappa_{chem}$  is slightly higher than  $\kappa_{gf}$  during early evening traffic rush hour and cooking time, when emissions of primary hydrophobic particles (e.g. BC and POA) are high (Fig. 3), thus resulting in a large percentage of externally-mixed particles). Causes of the overestimation in  $\kappa_{chem}$  during the traffic rush hour and cooking time will be discussed in the following paragraph. The particles experience rapid conversion and mixing in urban Beijing due to high precursor gases (Sun et al., 2015; Wu et al., 2016; Ren et al., 2018), thus the aged particles produced through photochemical processes in the afternoon can mix and interact with the freshly emitted primary particles from traffic and cooking sources (Wu et al., 2008). Therefore, during nighttime (22:00-06:00, LT), the particles are more uniform and internally-mixed, which is reflective of the assumption for calculation of  $\kappa_{chem}$ , a much better consistency between  $\kappa_{chem}$  and  $\kappa_{gf}$  is hence presented.



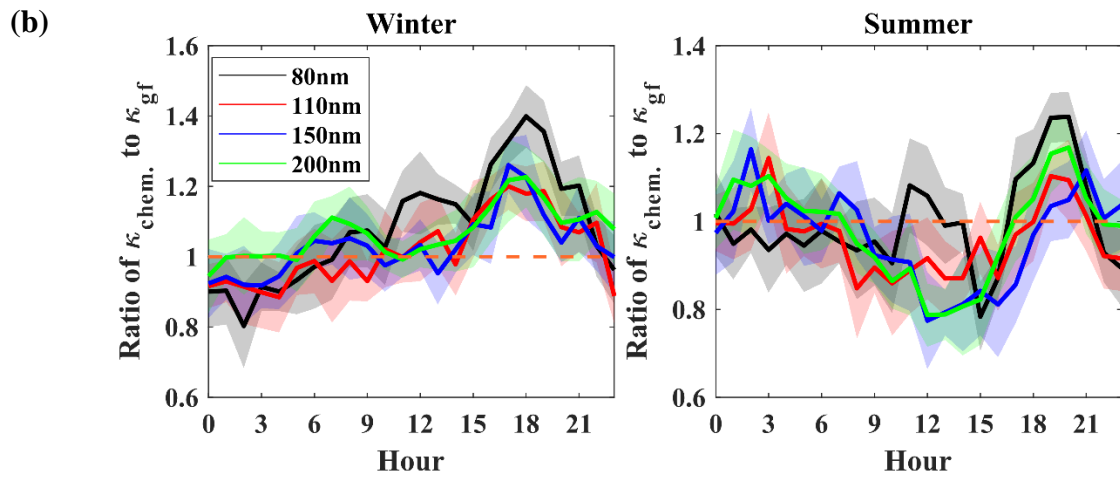
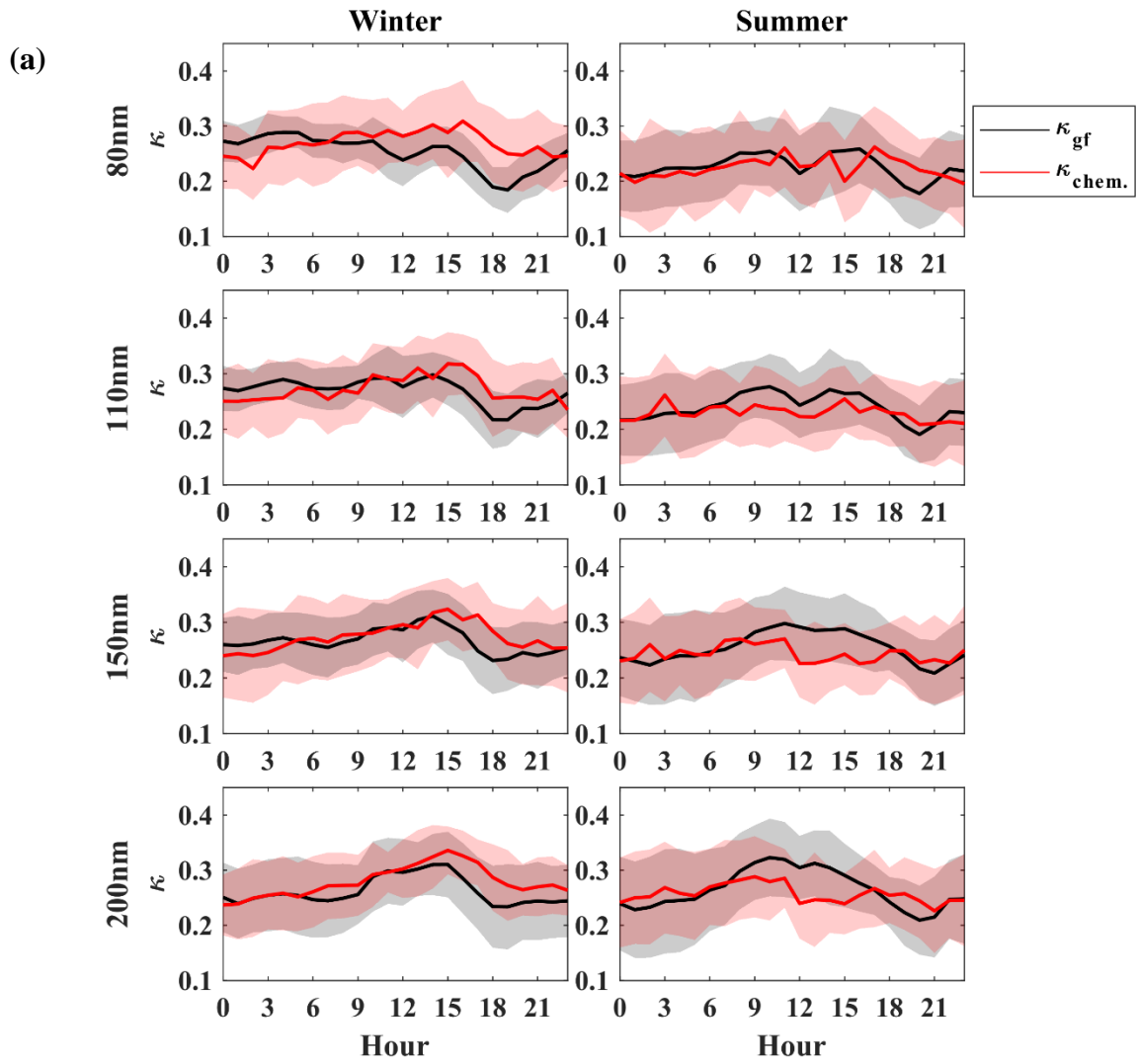
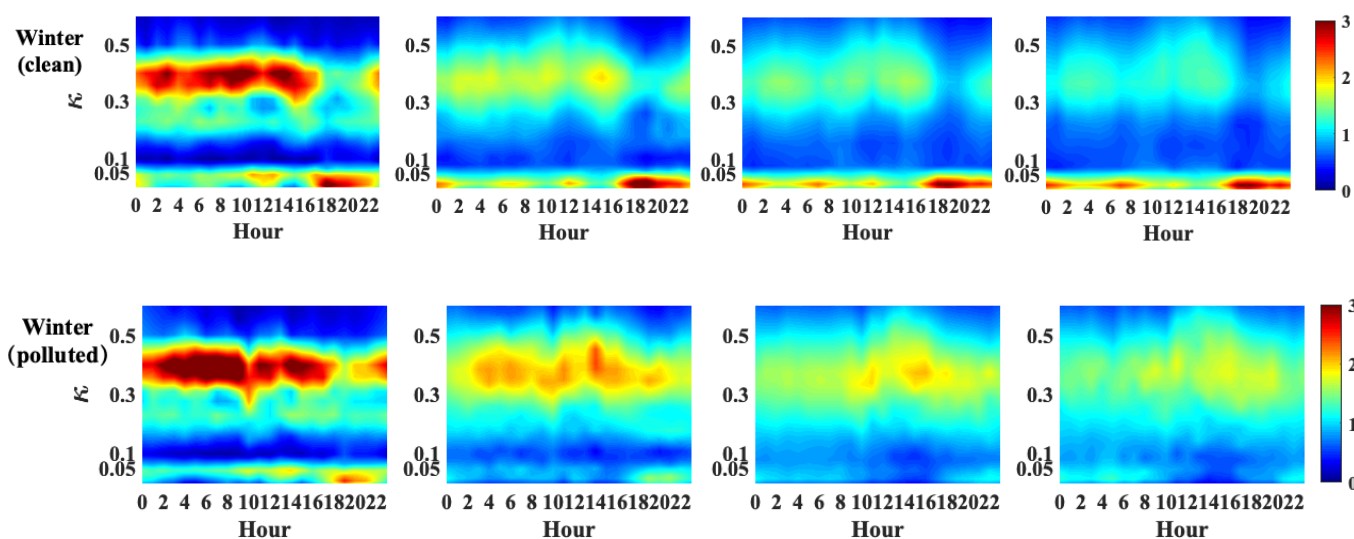


Figure 6. Diurnal variations of (a)  $\kappa_{\text{chem}}$  using size-resolved chemical composition data and  $\kappa_{\text{gf}}$  in winter and summer period; and (b) ratio of  $\kappa_{\text{chem}}$  to  $\kappa_{\text{gf}}$  in winter and summer period. The shade regions denote the error bars ( $1\sigma$ ).

318 In winter, the disparity between  $\kappa_{chem}$  to  $\kappa_{gf}$  is insignificant at 09:00-15:00 due to the weakening effect of  
 319 photochemical aging. From 15:00 to 21:00 LT, due to the strong vehicle and cooking sources around the site,  
 320 the particles are dominated by the hydrophobic mode with a large concentration of externally-mixed BC and  
 321 POA particles (Fig. 3), the calculated  $\kappa_{chem}$  is much higher than  $\kappa_{gf}$ , with the maximum ratio of  $\kappa_{chem}$  to  $\kappa_{gf}$  of  
 322 1.4, and the greatest disparity is observed for small particles. The disparity is further enhanced during clean  
 323 periods when the hydrophobic mode is dominant (Fig. 7, Fig. S1). Note that during the nighttime,  $\kappa_{chem}$  is  
 324 slight lower than  $\kappa_{gf}$ , with the minimum ratio of  $\kappa_{chem}$  to  $\kappa_{gf}$  of  $\sim 0.8$  for 80 nm particles and  $\sim 0.9$  for 110 and  
 325 150 nm particles at 02:00-04:00 LT (Fig. 6b), indicating an underestimation of particle hygroscopicity using  
 326 composition data. The disparity at nighttime is further increased during heavily polluted events (Fig. S1),  
 327 when the particles are more internally-mixed with only one hygroscopic mode (Fig. 7). We propose the  
 328 increased underestimation during polluted conditions is likely due to enhanced condensation of secondary  
 329 hygroscopic compounds (e.g. nitrate, sulfate, SOA) on pre-existing aerosols at lower temperature and or  
 330 hydrophilic SOA formation under higher relative humidity at nighttime (Wu et al., 2008; Wang et al., 2016;  
 331 An et al., 2019). However, such condensation effect during nighttime is less significant (indicated by the  
 332 smaller disparity between  $\kappa_{chem}$  and  $\kappa_{gf}$ ) than the aging effect caused by aerosols photochemical processes  
 333 around noontime (Peng et al., 2016b).



334  
 335  
 336 Figure 7. Diurnal cycles of  $\kappa_{gf}$ -PDF for 80, 110, 150 and 200 nm particles in clean and polluted events in  
 337 winter.

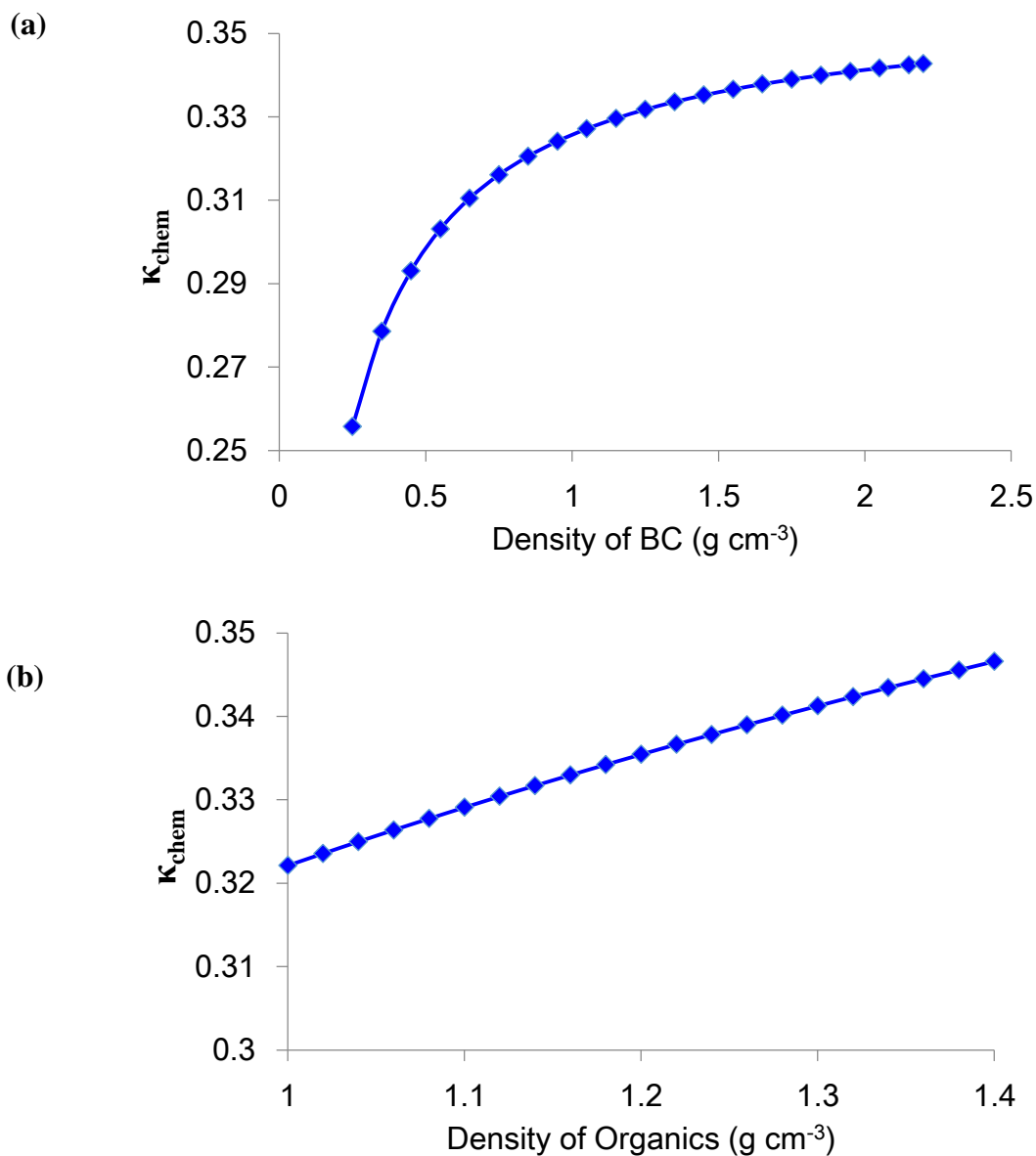
339 We suppose that the higher/lower  $\kappa_{chem}$  should be firstly closely associated with temporal changes in  
340 actual effective density of BC with the particles aging/diurnal variations of local emissions. It has been  
341 demonstrated that rapid aging of BC can occur over a few hours in the polluted urban area (Peng et al.,  
342 2016b). The externally-mixed BC particles are with fractal structure and chain-like aggregates and have  
343 been reported with effective density of 0.25-0.45 g cm<sup>-3</sup>(McMurry et al., 2002), while the BC particles in the  
344  $\kappa_{chem}$  calculation is assumed as void free with effective density of 1.7 g cm<sup>-3</sup>. This leads to less BC volume  
345 fraction than it actually is and thus the greater  $\kappa_{chem}$  during the traffic rush hour and cooking time when BC  
346 particles are mostly freshly emitted with uncompacted structure. In addition, the significant increase in  
347 volume fraction of POA during the late afternoon would result in changes of composition of organic  
348 aerosols and thereby a density much closer to that of POA than the assumed one (1.2 g cm<sup>-3</sup>) in the  
349 calculation should be applied. A sensitivity test has been done to examine the effect of density of BC and  
350 organics on calculated  $\kappa_{chem}$  (Fig. 8). The result shows that the  $\kappa_{chem}$  value can be reduced by 16-33% by  
351 decreasing the BC effective density from 1.7 g cm<sup>-3</sup> to 0.25-0.45 g cm<sup>-3</sup>. This basically explains the disparity  
352 between  $\kappa_{chem}$  and  $\kappa_{gf}$  during the traffic rush hour when a large amount of BC is freshly emitted. The changes  
353 in  $\kappa_{chem}$  are within  $\pm 4\%$  by varying the organic density from 1.2 (mixture of SOA and POA) to 1.0  
354 (typically for POA) or 1.4 g cm<sup>-3</sup> (typically for SOA) (Zamora et al., 2019), showing much less impacts of  
355 variations of organic density on  $\kappa_{chem}$ . In conclusion, the result demonstrated that the disparity between  $\kappa_{chem}$   
356 and  $\kappa_{gf}$  during late afternoon in winter is largely due to the inappropriate use of the BC particles density that  
357 is closely associated with its morphology or degree of its aging. Our study suggest that, to accurately  
358 parameterize the effect of BC aging on particles hygroscopicity, it is critical to measure the effective density  
359 and morphology of ambient BC, in particularly in those regions with complex influences of rapid secondary  
360 conversion/aging processes and local sources.

361 In that way, the lower  $\kappa_{chem}$  value derived around noontime in summer, when BC aerosols may be more  
362 compact through strong photochemical aging, is probably due to application of a lower BC density in the  
363 calculation. However, the sensitivity test indicates that, to fill the gap between  $\kappa_{chem}$  and  $\kappa_{gf}$  observed at  
364 noontime in summer, the effective density of BC should be extremely high due to decreased sensitivity of

365  $\kappa_{chem}$  to BC density with its aging. In this case, the density of BC has been assumed as  $1.7 \text{ g cm}^{-3}$ , which  
366 reflects a very compacted and void free structure of the BC particles. This currently applied value represents  
367 an upper limit for the effective density of ambient BC particles according to previous observations near or in  
368 Beijing (Zhang et al., 2015), which suggested the aged BC is generally with effective density of 1.2-1.4  $\text{g cm}^{-3}$ .  
369 Using these ambient observed values would lead to further underestimation in  $\kappa_{chem}$ . In addition, the  
370 photochemical aging can change the overall effective density of organic aerosols through changing their  
371 chemical composition. However, the effective density of the photochemical oxidized organic particles (e.g.  
372 SOA) does not change much on the timescale of several hours, and was observed ranging between 1.2 and  
373  $1.3 \text{ g cm}^{-3}$  (Bahreini et al., 2005). It can only explain ~4% at most of the underestimation in  $\kappa_{chem}$  around  
374 noontime in summer by applying a density value of  $1.4 \text{ g cm}^{-3}$  (typically for SOA). Therefore, application of  
375 higher densities of BC and organics in the calculation cannot fully explain the disparity between  $\kappa_{chem}$  and  
376  $\kappa_{gf}$  during early afternoon in summer when strong photochemical processes are expected.

377 The uncertainty in calculation of  $\kappa_{chem}$  may be also related to the uncertainty caused by hygroscopic  
378 parameter of organics that vary widely over a range of diverse constituents of SOA (Suda et al., 2012). The  
379 lower  $\kappa_{chem}$  indicates that the  $\kappa$  of secondary organic aerosols formed through the strong photochemical  
380 oxidation processes in summer of urban Beijing are likely underestimated. In this study, the mean  $\kappa$  value of  
381 organics derived from the  $f_{44}$  parametrized equation is  $0.20 \pm 0.02$ , ranging from 0.17 to 0.23 during  
382 09:00-17:00. While the organic aerosols, especially for particles in accumulated mode, may be more  
383 hydrophilic with much larger  $\kappa$ , i.e.  $>0.2$  due to large formation of highly-oxidized OA. One can easily get  
384 that increasing the  $\kappa$  of organic aerosols from 0.2 to 0.3 can explain about 11-13% underestimation of  $\kappa_{chem}$ ,  
385 but representing an upper limit of the impact of hygroscopicity of organic aerosols on the calculation. This is  
386 because that the  $\kappa$  value of 0.3 corresponds to the maximum possible for ambient organic aerosols.  
387 Additionally, the  $f_{44}$  parametrized equation tends to overestimate the  $\kappa$  according to Fröhlich et al. (2015),  
388 which should yield a larger  $\kappa_{chem}$ . Finally, the coexisting hygroscopic and hydrophobic species may have a  
389 strong influence on the phase state of particles, also likely affecting chemical interactions between inorganic  
390 and organic compounds as well as the overall hygroscopicity of mixed particles (Peng et al., 2016a). Overall,

391 The lower  $\kappa_{chem}$  caused by the photochemical aging effect is likely resulted from multiple impacts of  
392 inappropriate application of density and hygroscopic parameter of organic aerosols in the calculation, as  
393 well as the influences from chemical interaction between organic and inorganic compounds on the overall  
394 hygroscopicity of mixed particles. This topic warrants further investigations.



398 Figure 8. Sensitivity of  $\kappa_{chem}$  to variations of density of BC (a) and organics (b)

### 399 3.5. Observation from other stations

399 The aging process in the summer period is related to photochemical processing in strong solar radiation  
400 conditions. The photochemical reactions produce sulfate and secondary organic aerosol, condensing on the  
401 surface of slightly- or non-hygroscopic primary aerosols (such as BC) (Zhang et al., 2008). To confirm such

402 photochemical aging effect on particle hygroscopicity, we further examine the diurnal variations of  $\kappa_{chem}$  and  
403  $\kappa_{gf}$  or  $\kappa_{CCNc}$  (only at XZ site) based on observations in summer at two other sites in north China (Fig. 1). The  
404 XT site is located in the suburb of XT city, which is about 400 km south of Beijing, with high levels of  
405 industrialization and urbanization. Due to industrial emissions and typically weak ventilating winds,  
406 concentrations of  $PM_{2.5}$ , black carbon and gaseous precursors are usually high at the site (Fu et al., 2014).  
407 Xinzhou is located in north of Taiyuan and about 360 km southwest of Beijing, and is surrounded by  
408 mountains on three sides. Local emissions from motor vehicles and industrial activities have relatively little  
409 influence on the sampled aerosol (Zhang et al., 2016). Because of its location and elevation, the aerosol at  
410 the XZ site is usually aged and transported from other areas. The sampling period was from July 22 to  
411 August 26, 2014 and from May 17 to June 14, 2016 at XZ and XT site respectively.

412 We find that the case at the XT site is very similar to that observed in BJ (Fig. 9a), with a lower  $\kappa_{chem}$   
413 than  $\kappa_{gf}$  around noon time. But, because of much less influences from the local sources at XT compared to  
414 that at BJ, such underestimation by  $\kappa_{chem}$  continued until night at XT (Fig. 9b). Interestingly, a noontime  
415 lower  $\kappa_{chem}$  was not observed in the diurnal cycles at the XZ site, where  $\kappa_{chem}$  and  $\kappa_{CCNc}$  had similar diurnal  
416 patterns (Fig. 9c) with a roughly constant ratio of  $\kappa_{chem}$  to  $\kappa_{CCNc}$  of  $\sim 0.8-0.9$  (Fig. 9d). This is probably  
417 because the XZ site is usually the recipient of aerosols transported from other areas that are already aged and  
418 well-mixed, with minimal impact of further aging (Zhang et al., 2017). Also, the rate of oxidation and  
419 condensation may be slow in the relatively remote area where the gas precursors and oxidants are not as  
420 high as they are closer to sources regions. But at XT, which is located in the heavily polluted area in the  
421 north China Plain (Fu et al., 2014), aerosol emissions and processing are more similar to that in urban  
422 Beijing. These observations from other sites further confirms the the photochemical aging effect that will  
423 largely underestimate the particles hygroscopicity using simple mixing rule based on chemical composition.

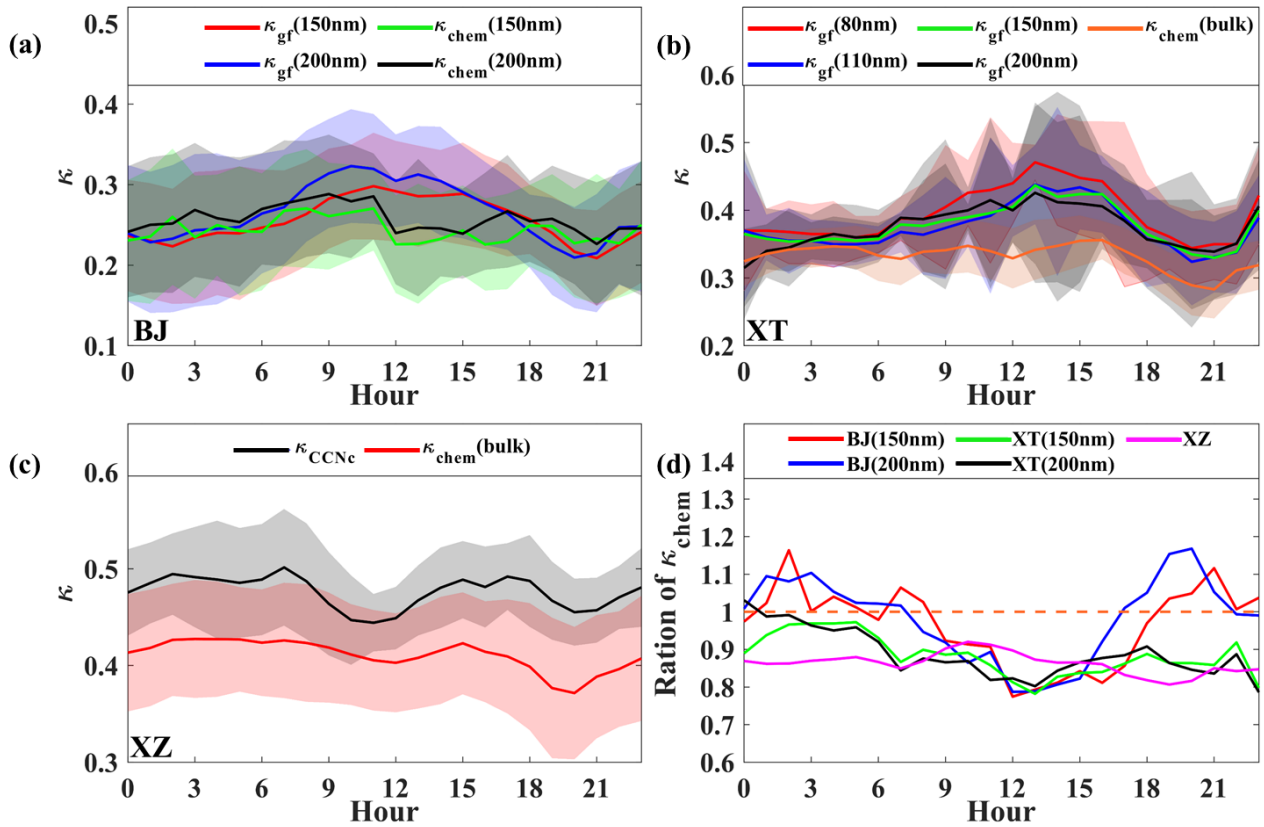


Figure 9. Diurnal variations in (a)  $\kappa_{chem}$  and  $\kappa_{gf}$  for 150 and 200 nm particles at BJ site; (b)  $\kappa_{chem}$  and  $\kappa_{gf}$  for 40, 80, 110, 150 and 200 nm particles at XT site; (c)  $\kappa_{chem}$  and mean  $\kappa_{CCNC}$  for particles at XZ site, and (d) ratio of mean  $\kappa_{chem}$  to  $\kappa_{gf}$  at the three sites.

#### 4. Conclusion

Using measurements of aerosol composition and hygroscopicity made in Beijing (BJ) during a winter period of 2016 and a summer period of 2017, this paper analyzes the daily variation and seasonal differences of size-resolved aerosol hygroscopicity in urban Beijing. We mainly focus on studying the disparity of  $\kappa_{gf}$  and  $\kappa_{chem}$  between summer and winter to reveal the impact of atmospheric processes and mixing state of the particles on its hygroscopicity. The uncertainty in calculating  $\kappa$  by using chemical composition with a uniform internal mixing hypothesis is elucidated from the diurnal variations of the difference between the calculated values: in summer, lower  $\kappa_{chem}$  is obtained around noontime, with a ratio of  $\kappa_{chem}$  to  $\kappa_{gf}$  of about 0.8-0.9 for large particles (i.e. 150 nm and 200 nm), showing an underestimation of particles hygroscopicity by using simple mixing rule based on chemical composition. Combining with the observation from XT and XZ, we attribute the underestimation to the rapid noontime photochemical aging processes in summer,

439 which induces the aging effect that will lead to a lower  $\kappa$  if assuming a uniform mixing of the particles. The  
440 lower  $\kappa_{chem}$  is likely resulted from multiple impacts of inappropriate application of density and hygroscopic  
441 parameter of organic aerosols in the calculation, as well as the unknown influences from chemical  
442 interaction between organic and inorganic compounds on the overall hygroscopicity of mixed particles.

443 In winter, larger  $\kappa_{chem}$  than  $\kappa_{gf}$  for >100 nm particles is derived around noontime and in the early  
444 afternoon, with the maximum ratio of  $\kappa_{chem}$  to  $\kappa_{gf}$  of 1.2-1.4 when the particles are dominated by the  
445 hydrophobic mode with a large number of externally-mixed POA particles from strong vehicle and cooking  
446 sources. We attribute this large disparity between  $\kappa_{chem}$  and  $\kappa_{gf}$  to changes of BC morphology that can be  
447 indicated by effective density of BC. The sensitivity test shows that it can well explain the disparity during  
448 the traffic rush hour by applying BC effective density of 0.25-0.45 g cm<sup>-3</sup>. However, we suggest that, to  
449 accurately parameterize or account for the effect of BC density on particles hygroscopicity, future  
450 investigations need to measure the effective density of ambient BC, in particularity in those regions with  
451 complex local sources. Our results highlight the impacts of atmospheric processes, sources on aerosol  
452 mixing state and hygroscopicity, which should be quantified and considered in models for different  
453 atmospheric conditions.

454  
455 *Data availability.* All data needed to evaluate the conclusions in the paper are present in the paper and/or the  
456 Supplementary Materials. Also, all data used in the study are available from the corresponding author upon  
457 request (fang.zhang@bnu.edu.cn).

458 *Author contributions.* F.Z. and J. L conceived the conceptual development of the manuscript. X. F. directed  
459 and performed of the experiments with L.C., X.J., Y. W., and F. Z.. F.Z., J.L., and X.F. conducted the data  
460 analysis and wrote the draft of the manuscript, and all authors edited and commented on the various sections  
461 of the manuscript. J.L. and X.F. contribute equally to this work.

462 *Competing interests.* The authors declare no competing interests.

463 *Acknowledgements.* This work was funded by National Natural Science Foundation of China (NSFC)  
464 research projects (grant nos. 41975174, 41675141, 91544217), the National Key R&D Program of China  
465 (grant no. 2017YFC1501702). We thank all participants of the field campaign for their tireless work and



466 cooperation. We also would like to thank the two anonymous reviewers for their insightful and constructive  
467 comments.

## 468 **References**

- 469 An, Z., Huang, R. J., Zhang, R., Tie, X., Li, G., Cao, J., Zhou, W., Shi, Z., Han, Y., Gu, Z., and Ji, Y.:  
470 Severe haze in Northern China: A synergy of anthropogenic emissions and atmospheric processes,  
471 Proceedings of the National Academy of Sciences, 116(18), 8657–8666, doi:10.1073/pnas.1900125116,  
472 2019.
- 473 Bahreini, R., Keywood, M. D., Ng, N. L., Varutbangkul, V., and Jimenez, J. L.: Measurements of secondary  
474 organic aerosol from oxidation of cycloalkenes, terpenes, and *m*-xylene using an aerodyne aerosol mass  
475 spectrometer. Environ. Sci. Technol., 39(15), 5674–5688, 2005.
- 476 Bougiatioti, A., Fountoukis, C., Kalivitis, N., Pandis, S. N., Nenes, A., and Mihalopoulos, N.: Cloud  
477 condensation nuclei measurements in the marine boundary layer of the Eastern Mediterranean: CCN  
478 closure and droplet growth kinetics, Atmos. Chem. Phys., 9, 7053–7066, doi: 10.5194/acp-9-7053-2009,  
479 2009.
- 480 Carrico, C. M., M. D. Petters, S. M. Kreidenweis, J. L. Collett Jr., G. Engling, and Malm W. C.: Aerosol  
481 hygroscopicity and cloud droplet activation of extracts of filters from biomass burning experiments, J.  
482 Geophys. Res., 113, D08206, doi:10.1029/2007JD009274. 2008.
- 483 Cerully, K. M., Raatikainen, T., Lance, S., Tkacik, D., Tiitta, P., Petäjä T., Nenes, A. : Aerosol  
484 hygroscopicity and CCN activation kinetics in a boreal forest environment during the 2007 EUCAARI  
485 campaign, Atmos. Chem. Phys., 11, 12369–12386, doi: 10.5194/acp-11-12369-2011, 2011.
- 486 Chang, R.-W., Liu, P., Leaitch, W., and Abbatt, J.: Comparison between measured and predicted CCN  
487 concentrations at Egbert, Ontario: Focus on the organic aerosol fraction at a semi-rural site, Atmos.  
488 Environ., 41, 8172–8182, 2007.
- 489 Collins, D. R., Flagan, R. C., and Seinfeld, J. H.: Improved inversion of scanning DMA data, Aerosol Sci.  
490 Technol., 36(1), 1–9, 2002.

491 Cruz, C. N. and Pandis, S. N.: Deliquescence and hygroscopic growth of mixed inorganic-organic  
492 atmospheric aerosol, *Environ. Sci. Technol.*, 34, 4313–4319, doi: 10.1021/es9907109, 2000.

493 DeCarlo, P. F., Kimmel, J. R., Trimborn, A., Northway, M. J., Jayne, J. T., Aiken, A. C., Gonin, M., Fuhrer,  
494 K., Horvath, T., Docherty, K., Worsnop, D. R., and Jimenez, J. L.: Field-deployable, high-resolution,  
495 time-of-flight aerosol mass spectrometer, *Anal. Chem.*, 78, 8281–8289, doi: 10.1021/ac061249n, 2006.

496 Fors, E. O., Swietlicki, E., Svenningsson, B., Kristensson, A., Frank, G. P., and Sporre, M.: Hygroscopic  
497 properties of the ambient aerosol in southern Sweden – a two year study, *Atmos. Chem. Phys.*, 11, 8343–  
498 8361, doi: 10.5194/acp-11-8343-2011, 2011.

499 Fröhlich, R., Crenn, V., Setyan, A., Belis, C. A., Canonaco, F., Favez, O., Riffault, V., Slowik, J. G.,  
500 Aas, W., Aijälä M., Alastuey, A., Artiñano, B., Bonnaire, N., Bozzetti, C., Bressi, M., Carbone, C., Coz,  
501 E., Croteau, P. L., Cubison, M. J., Esser-Gietl, J. K., Green, D. C., Gros, V., Heikkinen, L., Herrmann, H.,  
502 Jayne, J. T., Lunder, C. R., Minguillón, M. C., Mocnik, G., O’Dowd, C. D., Ovadnevaite, J., Petralia, E.,  
503 Poulain, L., Priestman, M., Ripoll, A., Sarda-Estève, R., Wiedensohler, A., Baltensperger, U., Sciare, J.,  
504 and Prévôt, A. S. H.: ACTRIS ACSM intercomparison – Part 2: Intercomparison of ME-2 organic source  
505 apportionment results from 15 individual, co-located aerosol mass spectrometers, *Atmos. Meas. Tech.*, 8,  
506 2555–2576, doi:10.5194/amt-8-2555-2015, 2015.

507 Fu, G. Q., Xu, W. Y., Yang, R. F., Li, J. B., & Zhao, C. S. : The distribution and trends of fog and haze in  
508 the North China Plain over the past 30 years, *Atmos. Chem. Phys.*, 14, 11949–11958, doi:  
509 10.5194/acp-14-11949-2014, 2014.

510 Gasparini, R., R. Li, and D. R. Collins: Integration of size distributions and size-resolved hygroscopicity  
511 measured during the Houston Supersite for compositional categorization of the aerosol, *Atmos. Environ.*,  
512 38, 3285–3303, doi:10.1016/j.atmosenv.2004.03.019, 2004.

513 Good, N., Topping, D. O., Allan, J. D., Flynn, M., Fuentes, E., Irwin, M., Williams, P. I., Coe, H., and  
514 McFiggans, G.: Consistency between parameterisations of aerosol hygroscopicity and CCN activity  
515 during the RHaMBLe discovery cruise, *Atmos. Chem. Phys.*, 10, 3189–3203, doi:  
516 10.5194/acp-10-3189-2010, 2010.

517 Gunthe, S. S., King, S. M., Rose, D., Chen, Q., Roldin, P., Farmer, D. K., Jimenez, J. L., Artaxo, P., Andreae,  
518 M. O., Martin, S.T., and Pöschl, U.: Cloud condensation nuclei in pristine tropical rainforest air of  
519 Amazonia: size-resolved measurements and modeling of atmospheric aerosol composition and CCN  
520 activity, *Atmos. Chem. Phys.*, 9, 7551–7575, doi: 10.5194/acp-9-7551-2009, 2009.

521 Gysel, M., Crosier, J., Topping, D. O., Whitehead, J. D., Bower, K.N., Cubison, M. J., Williams, P. I., Flynn,  
522 M. J., McFiggans, G.B., and Coe, H.: Closure study between chemical composition and hygroscopic  
523 growth of aerosol particles during TORCH2, *Atmos. Chem. Phys.*, 7, 6131–6144, doi:  
524 10.5194/acp-7-6131-2007, 2007.

525 Gysel, M., McFiggans, G. B., and Coe, H.: Inversion of tandem differential mobility analyser (TDMA)  
526 measurements, *J. Aerosol Sci.*, 40, 134–151, doi: 10.1016/j.jaerosci.2008.07.013, 2009.

527 Hu, W., Hu, M., Hu, W., Jimenez, J. L., Yuan, B., Chen, W., Wang, M., Wu, Y., Chen, C., Wang, Z., Peng,  
528 J., Zeng, L., and Shao, M.: Chemical composition, sources, and aging process of submicron aerosols in  
529 Beijing: Contrast between summer and winter, *J. Geophys. Res.*, 121, 1955–1977, doi:  
530 10.1002/2015JD024020, 2016.

531 Irwin, M., Good, N., Crosier, J., Choularton, T. W., & McFiggans, G.: Reconciliation of measurements of  
532 hygroscopic growth and critical supersaturation of aerosol particles in central Germany *Atmos. Chem.*  
533 *Phys.*, 10, 11737–11752, doi:10.5194/acp-10-11737-2010, 2010.

534 Jacobson, M.Z. : Strong radiative heating due to the mixing state of black carbon in atmospheric aerosols,  
535 *Nature*, 409(6821):695-697, 2001.

536 Kulmala, M., Petaja, T., Monkkonen, P., Koponen, I.K., Dal Maso, M., Aalto, P.P., Lehtinen, K.E.J., and  
537 Kerminen, V.M. : On the growth of nucleation mode particles: source rates of condensable vapor in  
538 polluted and clean environments, *Atmos. Chem. Phys.*, 5, 409–416, doi: 10.5194/acp-5-409-2005, 2005.

539 Kuwata, M., Kondo, Y., Miyazaki, Y., Komazaki, Y., Kim, J. H., Yum, S. S., Tanimoto, H., and Matsueda,  
540 H.: Cloud condensation nuclei activity at Jeju Island, Korea in spring 2005, *Atmos. Chem. Phys.*, 8,  
541 2933–2948, doi:10.5194/acp-8-2933-2008, 2008.

542 Liu, D., Joshi, R., Wang, J., Yu, C., Allan, J. D., Coe, H., Flynn, M. J., Xie, C., Lee, J., Squires, F., Kotthaus,  
543 S., Grimmond, S., Ge, X., Sun, Y., and Fu, P.: Contrasting physical properties of black carbon in urban

544 Beijing between winter and summer, *Atmos. Chem. Phys. Discuss.*, doi: 10.5194/acp-2018-1142, in  
545 review, 2018.

546 Liu, P. F., Zhao, C. S., Göbel, T., Hallbauer, E., Nowak, A., Ran, L., Xu, W. Y., Deng, Z. Z., Ma, N.,  
547 Mildenerger, K., Henning, S., Stratmann, F., and Wiedensohler, A.: Hygroscopic properties of aerosol  
548 particles at high relative humidity and their diurnal variations in the North China Plain, *Atmos. Chem.  
549 Phys.*, 3479–3494, doi:10.5194/acp-11-3479-2011, 2011.

550 Ma, Y., Brooks, S. D., Vidaurre, G., Khalizov, A. F., Wang, L., and Zhang, R.: Rapid modification of  
551 cloud-nucleating ability of aerosols by biogenic emissions, *Geophys. Res. Lett.*, 40, 6293–6297, doi:  
552 10.1002/2013GL057895, 2013.

553 Massling, A., Stock, M., and Wiedensohler, A.: Diurnal, weekly, and seasonal variation of hygroscopic  
554 properties of submicrometer urban aerosol particles, *Atmos. Environ.*, 39(21), 3911–3922, doi:  
555 10.1016/j.atmosenv.2005.03.020, 2005.

556 McMurry, P. H.; Wang, X.; Park, K.; Ehara, K. The Relationship between Mass and Mobility for  
557 Atmospheric Particles. *Aerosol Sci. Technol.*, 36, 227-238, 2002.

558 Mei, F., Hayes, P. L., Ortega, A. M., Taylor, J. W., Allan, J. D., Gilman, J. B., Kuster, W. C., de Gouw, J. A.,  
559 Jimenez, J. L., and Wang, J.: Droplet activation properties of organic aerosols observed at an urban site  
560 during CalNex-LA, *J. Geophys. Res.*, 118, 2903–2917, doi: 10.1002/jgrd.50285, 2013.

561 Mikhailov, E. F., Mironov, G. N., Pöhlker, C., Chi, X., Krüger, M. L., Shiraiwa, M., Förster, J. D., Pöschl,  
562 U., Vlasenko, S. S., Ryshkevich, T. I., Weigand, M., Kilcoyne, A. L. D., and Andreae, M. O.: Chemical  
563 composition, microstructure, and hygroscopic properties of aerosol particles at the Zotino Tall Tower  
564 Observatory (ZOTTO), Siberia, during a summer campaign, *Atmos. Chem. Phys.*, 15, 8847–8869,  
565 doi:10.5194/acp-15-8847-2015, 2015.

566 Peng, C., Jing, B., Guo, Y. C., Zhang, Y. H., and Ge, M. F.: Hygroscopic behavior of multicomponent  
567 aerosols involving nacl and dicarboxylic acids. *J. Phys. Chem. A*, 120(7), 1029-1038, 2016a.

568 Peng, J. F., Hu, M., Guo, S., Du, Z., Shang, D., and Zheng, J.: Ageing and hygroscopicity variation of black  
569 carbon particles in Beijing measured by a quasi-atmospheric aerosol evolution study (quality) chamber.  
570 *Atmospheric Chemistry and Physics*, 17(17), 10333-10348, 2017a.

571 Peng, J. F., Hu, M., Du, Z. F., Wang, Y. H., Zheng, J., Zhang, W. B., Yang, Y. D., Qin, Y. H., Zheng, R.,  
572 Xiao, Y., Wu, Y. S., Lu, S. H., Wu, Z. J., Guo, S., Mao, H. J., and Shuai, S. J.: Gasoline aromatics: a  
573 critical determinant of urban secondary organic aerosol formation, *Atmospheric Chemistry and Physics*,  
574 17, 10743-10752, 2017b.

575 Peng, J. F., Hu, M., Wang, Z. B., Huang, X. F., Kumar, P., Wu, Z. J., Guo, S., Yue, D. L., Shang, D. J.,  
576 Zheng, Z., and He, L. Y.: Submicron aerosols at thirteen diversified sites in China: size distribution, new  
577 particle formation and corresponding contribution to cloud condensation nuclei production, *Atmospheric*  
578 *Chemistry and Physics*, 14, 10249-10265, DOI 10.5194/acp-14-10249-2014, 2014.

579 Peng, J. F., Hu, M., Guo, S., Du, Z. F., Zheng, J., Shang, D. J., Zamora, M. L., Zeng, L. M., Shao, M., Wu,  
580 Y. S., Zheng, J., Wang, Y., Glen, C. R., Collins, D. R., Molina, M. J., and Zhang, R. Y.: Markedly  
581 enhanced absorption and direct radiative forcing of black carbon under polluted urban environments, *P*  
582 *Natl Acad Sci USA*, 113, 4266-4271, 10.1073/pnas.1602310113, 2016b.

583 Petters, M. D. and Kreidenweis, S. M.: A single parameter representation of hygroscopic growth and cloud  
584 condensation nucleus activity, *Atmos. Chem. Phys.*, 7, 1961–1971, doi: 10.5194/acp-7-1961-2007, 2007.

585 Ren, J. Y., Zhang, F., Wang, Y. Y., Collins, D., Fan, X. X., Jin, X. A., Xu, W. Q., Sun, Y. L., Cribb, M., and  
586 Li, Z. Q.: Using different assumptions of aerosol mixing state and chemical composition to predict CCN  
587 concentrations based on field measurements in urban Beijing, *Atmos. Chem. Phys.*, 18, 6907–6921, doi:  
588 10.5194/acp-18-6907-2018, 2018.

589 Rose, D., Nowak, A., Achtert, P., Wiedensohler, A., Hu, M., Shao, M., Zhang, Y., Andreae, M. O., and  
590 Pöschl, U.: Cloud condensation nuclei in polluted air and biomass burning smoke near the mega-city  
591 Guangzhou, China – Part 1: Size-resolved measurements and implications for the modeling of aerosol  
592 particle hygroscopicity and CCN activity, *Atmos. Chem. Phys.*, 10, 3365–3383,  
593 <https://doi.org/10.5194/acp-10-3365-2010>, 2010.

594 Saarnio, K., Frey, A., Niemi, J. V., Timonen, H., Rönkkö, T., Karjalainen, P., Vestenius, M., Teinilä, K.,  
595 Pirjola, L., Niemelä, V., Keskinen, J., Häyrinen, A., and Hillamo, R.: Chemical composition and size of  
596 particles in emissions of coal-fired power plant with flue gas desulphurization, *J. Aerosol Sci.*, 73, 14–26,  
597 2014.

598 Schill, S. R., Collins, D. B., Lee, C., Morris, H. S., Novak, G. A., and Prather, K. A.: The impact of aerosol  
599 particle mixing state on the hygroscopicity of sea spray aerosol. *ACS Central Science*, 1(3), 132-141,  
600 2015

601 Sjogren, S., Gysel, M., Weingartner, E., Baltensperger, U., Cubison, M. J., Coe, H., Zardini, A. A., Marcolli,  
602 C., Krieger, U. K., and Peter, T.: Hygroscopic growth and water uptake kinetics of two-phase aerosol  
603 particles consisting of ammonium sulfate, adipic and humic acid mixtures, *J. Aerosol Sci.*, 38, 157–171,  
604 doi: 10.1016/j.jaerosci.2006.11.005, 2007.

605 Suda, S. R., Petters, M. D., Matsunaga, A., Sullivan, R. C., Ziemann, P. J., and Kreidenweis, S. M.:  
606 Hygroscopicity frequency distributions of secondary organic aerosols. *J. Geophys. Res.*, 117(D4), D04207,  
607 2012

608 Svenningsson, B., Rissler, J., Swietlicki, E., Mircea, M., Bilde, M., Facchini, M. C., Decesari, S., Fuzzi, S.,  
609 Zhou, J., Mønster, J., and Rosenørn, T.: Hygroscopic growth and critical supersaturations for mixed  
610 aerosol particles of inorganic and organic compounds of atmospheric relevance, *Atmos. Chem. Phys.*, 6,  
611 1937–1952, doi: 10.5194/acp-6-1937-2006, 2006.

612 Sun, Y. L., Wang, Z. F., Du, W., Zhang, Q., Wang, Q. Q., Fu, P. Q., Pan, X. L., Li, J., Jayne, J., and  
613 Worsnop, D. R.: Long-term real-time measurements of aerosol particle composition in Beijing, China:  
614 Seasonal variations, meteorological effects, and source analysis, *Atmos. Chem. Phys.*, 15, 10149–10165,  
615 doi: 10.5194/acp-15-10149-2015, 2015.

616 Sun, Y., Du, W., Fu, P., Wang, Q., Li, J., Ge, X., Zhang, Q., Zhu, C., Ren, L., Xu, W., Zhao, J., Han, T.,  
617 Worsnop, D. R., and Wang, Z.: Primary and secondary aerosols in Beijing in winter: sources, variations  
618 and processes, *Atmos. Chem. Phys.*, 16, 8309–8329, doi: 10.5194/acp-16-8309-2016, 2016.

619 Swietlicki, E., Hansson, H. C., Hämeri, K., Svenningsson, B., Massling, A., McFiggans, G., McCurry, P.  
620 H., PetÄJÄ, T., Tunved, P., Gysel, M., Topping, D., Weingartner, E., Baltensperger, U., Rissler, J.,  
621 Wiedensohler, A., and Kulmala, M.: Hygroscopic properties of submicrometer atmospheric aerosol  
622 particles measured with H-TDMA instruments in various environments - a review, *Tellus B*, 60, 432–469,  
623 doi: 10.1111/j.1600-0889.2008.00350.x, 2008.

624 Tan, H., Xu, H., Wan, Q., Li, F., Deng, X., Chan, P. W., Xia, D., and Yin, Y.: Design and application of an  
625 unattended multifunctional H-TDMA system, *J. Atmos. Ocean. Tech.*, 30, 1136–1148, doi:  
626 10.1175/JTECH-D-12-00129.1, 2013.

627 Turpin, B. J. and Lim, H. J.: Species contributions to PM<sub>2.5</sub> mass concentrations: Revisiting common  
628 assumptions for estimating organic mass, *Aerosol Sci. Tech.*, 35, 602–610, doi:  
629 10.1080/02786820152051454, 2001.

630 Wang, J., Cubison, M. J., Aiken, A. C., Jimenez, J. L., and Collins, D. R.: The importance of aerosol mixing  
631 state and size-resolved composition on CCN concentration and the variation of the importance with  
632 atmospheric aging of aerosols, *Atmos. Chem. Phys.*, 10, 7267–7283, doi:10.5194/acp-10-7267-2010,  
633 2010.

634 Wang, J., Zhang, Q., Chen, M.-D., Collier, S., Zhou, S., Ge, X., Xu, J., Shi, J., Xie, C., Hu, J., Ge, S., Sun,  
635 Y., and Coe, H.: First chemical characterization of refractory black carbon aerosols and associated  
636 coatings over the Tibetan Plateau (4730 m a.s.l), *Environ. Sci. Tech.*, 51, 14072,  
637 doi:10.1021/acs.est.7b03973, 2017.

638 Wang, Q., Zhao, J., Du, W., Ana, G., Wang, Z., Sun, L., Wang, Y., Zhang, F., Li, Z., Ye, X., and Sun, Y.:  
639 Characterization of submicron aerosols at a suburban site in central China, *Atmos. Environ.*, 131, 115–  
640 123, doi:10.1016/j.atmosenv.2016.01.054, 2016.

641 Wang, S. C. and Flagan, R. C.: Scanning Electrical Mobility Spectrometer, *Aerosol Sci. Tech.*, 13, 230–240,  
642 1990.

643 Wang, Y., Zhang, F., Li, Z., Tan, H., Xu, H., Ren, J., Zhao, J., Du, W., and Sun, Y.: Enhanced  
644 hydrophobicity and volatility of submicron aerosols under severe emission control conditions in Beijing,  
645 *Atmos. Chem. Phys.*, 17, 5239–5251, doi: 10.5194/acp-17-5239-2017, 2017.

646 Wang Y., Li Z., Zhang Y., Du W., Zhang F., Tan H., Xu H., Fan T., Jin X., Fan X., Dong Z., Wang Q. and  
647 Sun Y.: Characterization of aerosol hygroscopicity, mixing state, and CCN activity at a suburban site in  
648 the central North China Plain, *Atmos. Chem. Phys.*, 18, 11739–11752, doi: 10.5194/acp-18-11739-2018,  
649 2018a.

- 650 Wang, Y., Z. Wu, N. Ma, Y. Wu, L. Zeng, C. Zhao, and A. Wiedensohler: Statistical analysis and  
651 parameterization of the hygroscopic growth of the sub-micrometer urban background aerosol in Beijing,  
652 *Atmos. Environ.*, 175, 184-191, doi: 10.1016/j.atmosenv.2017.12.003, 2018b.
- 653 Wex, H., Petters, M. D., Carrico, C. M., Hallbauer, E., Massling, A., McMeeking, G. R., Poulain, L., Wu, Z.,  
654 Kreidenweis, S. M., and Stratmann, F.: Towards closing the gap between hygroscopic growth and  
655 activation for secondary organic aerosol: Part 1—Evidence from measurements, *Atmos. Chem. Phys.*, 9,  
656 3987–3997, doi: 10.5194/acp-9-3987-2009, 2009
- 657 Wu, Z., Hu, M., Lin, P., Liu, S., Wehner, B., and Wiedensohler, A.: Particle number size distribution in the  
658 urban atmosphere of Beijing, China, *Atmos. Environ.*, 42, 7967–7980, doi:  
659 10.1016/j.atmosenv.2008.06.022, 2008.
- 660 Wu, Z. J., Poulain, L., Henning, S., Dieckmann, K., Birmili, W., Merkel, M., van Pinxteren, D., Spindler, G.,  
661 Müller, K., Stratmann, F., Herrmann, H., and Wiedensohler, A.: Relating particle hygroscopicity and  
662 CCN activity to chemical composition during the HCCT-2010 field campaign, *Atmos. Chem. Phys.*, 13,  
663 7983–7996, doi: 10.5194/acp-13-7983-2013, 2013.
- 664 Wu, Z. J., Zheng, J., Shang, D. J., Du, Z. F., Wu, Y. S., Zeng, L. M., Wiedensohler, A., and Hu, M.: Particle  
665 hygroscopicity and its link to chemical composition in the urban atmosphere of Beijing, China, during  
666 summertime, *Atmos. Chem. Phys.*, 16, 1123–1138, doi: 10.5194/acp-16-1123-2016, 2016.
- 667 Xu, W. Q., Sun, Y. L., Chen, C., Du, W., Han, T. T., Wang, Q. Q., Fu, P. Q., Wang, Z. F., Zhao, X. J., Zhou,  
668 L. B., Ji, D. S., Wang, P. C., and Worsnop, D. R.: Aerosol composition, oxidation properties, and sources  
669 in Beijing: results from the 2014 Asia-Pacific Economic Cooperation summit study, *Atmos. Chem. Phys.*,  
670 15, 13681–13698, doi: 10.5194/acp-15-13681-2015, 2015.
- 671 Ye, X., Tang, C., Yin, Z., Chen, J., Ma, Z., Kong, L., Yang, X., Gao, W., and Geng, F.: Hygroscopic growth  
672 of urban aerosol particles during the 2009 Mirage-Shanghai Campaign, *Atmos. Environ.*, 64, 263–269,  
673 doi: 10.1016/j.atmosenv.2012.09.064, 2013.
- 674 Zamora, M. L., Peng, J., Hu, M., Guo, S., Marrero-Ortiz, W., Shang, D., Zheng, J., Du, Z., Wu, Z., and  
675 Zhang, R.: Wintertime aerosol properties in Beijing, *Atmos. Chem. Phys.*, 19, 14329–14338,  
676 <https://doi.org/10.5194/acp-19-14329-2019>, 2019.



677 Zardini, A. A., Sjogren, S., Marcolli, C., Krieger, U. K., Gysel, M., Weingartner, E., Baltensperger, U., and  
678 Peter, T.: A combined particle trap/HTDMA hygroscopicity study of mixed in-organic/organic aerosol  
679 particles, *Atmos. Chem. Phys.*, 8, 5589–5601, doi:10.5194/acp-8-5589-2008, 2008

680 Zhang, F., Li, Y., Li, Z., Sun, L., Li, R., Zhao, C., Wang, P., Sun, Y., Liu, X., Li, J., Li, P., Ren, G., and Fan,  
681 T.: Aerosol hygroscopicity and cloud condensation nuclei activity during the AC3Exp campaign:  
682 Implications for cloud condensation nuclei parameterization, *Atmos. Chem. Phys.*, 14, 13423–13437, doi:  
683 10.5194/acp-14-13423-2014, 2014.

684 Zhang, F., Li, Z., Li, Y., Sun, Y., Wang, Z., Li, P., Sun, L., Wang, P., Cribb, M., Zhao, C., Fan, T., Yang, X.,  
685 and Wang, Q.: Impacts of organic aerosols and its oxidation level on CCN activity from measurement at a  
686 suburban site in China, *Atmos. Chem. Phys.*, 16, 5413–5425, doi: 10.5194/acp-16-5413-2016, 2016.

687 Zhang, F., Wang, Y., Peng, J., Ren, J., Zhang, R., Sun, Y., Collin, D., Yang, X., and Li, Z.: Uncertainty in  
688 predicting CCN activity of aged and primary aerosols, *J. Geophys. Res.-Atmos.*, 122, 11723–11736, doi:  
689 10.1002/2017JD027058, 2017.

690 Zhang, R., Khalizov, A. F., Pagels, J., Zhang, D., Xue, H., and McMurry, P. H.: Variability in morphology,  
691 hygroscopicity, and optical properties of soot aerosols during atmospheric processing, *PNAS*, 105(30),  
692 10291–10296, doi:10.1073/pnas.0804860105, 2008.

693 Zhang, R., Wang, G., Guo, S., Zamora, M. and Wang, Y.: Formation of urban fine particulate matter.  
694 *Chemical Reviews*, 115(10), 3803-3855, 2015

695 Zhang, Y., Zhang, Q., Cheng, Y., Su, H., Kecorius, S., Wang, Z., Wu, Z., Hu, M., Zhu, T., Wiedensohler, A.,  
696 and He, K.: Measuring the morphology and density of internally mixed black carbon with SP2 and  
697 VTDMA: new insight into the absorption enhancement of black carbon in the atmosphere, *Atmos. Meas.*  
698 *Tech.*, 9, 1833-1843, 2016.

699 Zhao, J., Du, W., Zhang, Y., Wang, Q., Chen, C., Xu, W., Han, T., Wang, Y., Fu, P., Wang, Z., Li, Z., and  
700 Sun, Y.: Insights into aerosol chemistry during the 2015 China Victory Day parade: results from  
701 simultaneous measurements at ground level and 260 m in Beijing, *Atmos. Chem. Phys.*, 17, 3215–3232,  
702 doi: 10.5194/acp-17-3215-2017, 2017.